Draft version June 11, 2020
Typeset using LaTeX **twocolumn** style in AASTeX63

On the existence of shear–current effects in magnetized burgulence

Maarit J. Käpylä,[1,2,3] Javier Álvarez Vizoso,[2] Matthias Rheinhardt,[1] Axel Brandenburg,[3,4,5] Petri Käpylä,[6] and Nishant K. Singh[7,2]

[1]Department of Computer Science, Aalto University, PO Box 15400, FI-00076 Aalto, Finland
[2]Max Planck Institute for Solar System Research, Justus-von-Liebig-Weg 3, D-37077 Göttingen, Germany
[3]Nordita, KTH Royal Institute of Technology and Stockholm University, Roslagstullsbacken 23, SE-10691 Stockholm, Sweden
[4]Department of Astronomy, AlbaNova University Center, Stockholm University, SE-10691 Stockholm, Sweden
[5]McWilliams Center for Cosmology & Department of Physics, Carnegie Mellon University, Pittsburgh, PA 15213, USA
[6]Georg-August-Universität Göttingen, Institut für Astrophysik, Friedrich-Hund-Platz 1, D 37077 Göttingen, Germany
[7]Inter-University Centre for Astronomy and Astrophysics, Post Bag 4, Ganeshkhind, Pune 411 007, India

(Dated: Revision: 1.285)

ABSTRACT

The possibility of explaining shear flow dynamos in terms of a magnetic shear–current (SC) effect is examined. A competing explanation is the incoherent α–shear dynamo effect. Our primary diagnostics is the determination of the turbulent magnetic diffusivity tensor, in particular the off-diagonal diffusivity tensor component η_{yx}, a systematically negative sign of which would imply coherent dynamo action through SC, in systems where the mean flow in the y direction has a constant x derivative. To be able to measure turbulent transport coefficients from systems with strong magnetic fluctuations, we present an extension of the test–field method (TFM) that is capable of such measurements in the case where the pressure gradient term is dropped from the MHD equations, which is a nonlinear TFM (NLTFM). The hydrodynamic equation is related to Burger's equation and the resulting flows are referred to as magnetized burgulence. We use both kinetic and magnetic forcings, to mimic cases without and with simultaneous small-scale dynamo action (SSD). When the simplified MHD flow is forced kinetically, negative η_{yx} values are obtained with exponential growth in both the radial and azimuthal magnetic field components. Using stochastic monochromatic magnetic forcing, the exponential growth is no longer seen, and NLTFM yields positive values of η_{yx}. In an attempt to recover the exponential growth seen in the kinetically forced case, we also employ an alternative forcing function with lowest k vectors being removed – in this case the exponential growth is recovered, but the NLTFM results do not change dramatically. Our analysis of the dynamo numbers for the coherent SC and incoherent α and SC effects show that the incoherent effects are the main drivers of the dynamo instability in majority of cases. The coherent SC effect is mildly enhancing the dynamo action in the kinetically forced cases, while we find no evidence for magnetic SC in our simulations.

1. INTRODUCTION

In recent years, the possibility of large-scale dynamo (LSD) action through the shear–current effect (Rogachevskii & Kleeorin 2003, 2004) in flows where more conventional dynamo effects, such as the α effect arising through stratification and rotation, cannot operate, has gained a lot of interest. In turbulence lacking helicity, say, due to the absence of rotation or stratification in density or turbulence intensity, the α tensor vanishes. The turbulent magnetic diffusivity tensor $\boldsymbol{\eta}$, however, is always found to have finite and positive diagonal components. Its off-diagonal components are in general also finite if there is rotation or shear. Rotation alone gives rise to the $\boldsymbol{\Omega}\times\boldsymbol{J}$ or Rädler effect (Rädler 1969a,b) and shear alone to the shear–current (SC) effect. For a suitable sign of the relevant off-diagonal component of $\boldsymbol{\eta}$, the latter can lead to dynamo action even without rotation, but the former would not without shear. Both the Rädler and SC effects have been discussed as additional or even major dynamo effects in stars (Pipin & Seehafer 2009), accretion disks (Lesur & Ogilvie 2008; Blackman 2010), and galactic magnetism (Chamandy & Singh 2018).

Astrophysical flows are also subject to vigorous small-scale dynamo (SSD) action, which should occur in any flow where the magnetic Reynolds and Prandtl numbers are large

Corresponding author: Maarit J. Käpylä
maarit.kapyla@aalto.fi

enough. The SSD produces strong, fluctuating magnetic fields at scales smaller than the forcing scale of the turbulence, on time scales short in comparison to the LSD instability (see, e.g., Brandenburg et al. 2012). Usually, the SSD is thought to be detrimental to α-effect driven dynamos, where dynamo action can be strongly suppressed in high Reynolds number regimes (e.g., Cattaneo & Vainshtein 1991; Vainshtein & Cattaneo 1992), unless the system can get a rid of small-scale magnetic helicity by interacting with its surroundings through helicity fluxes (e.g., Blackman & Field 2001; Brandenburg 2001; Brandenburg & Subramanian 2005). In the absence of magnetic background turbulence it has not yet been possible to verify the existence of a dynamo driven by the SC effect (Yousef et al. 2008; Brandenburg et al. 2008; Singh & Jingade 2015). Failure to understand the origin of large-scale magnetic fields in these numerical works in terms of the SC effect, together with the findings of significant α fluctuations in Brandenburg et al. (2008), provided enough motivation to explore the possibility of LSD action driven solely due to fluctuating α in shearing systems. Such an incoherent α–shear dynamo was studied analytically in a number of previous works, suggesting a possibility of generation of large-scale magnetic fields due to purely temporal fluctuations in α in the presence of shear (Heinemann et al. 2011; Mitra & Brandenburg 2012; Sridhar & Singh 2014).

It has, however, been claimed that in the presence of forcing in the induction equation, mimicking magnetic background turbulence provided, e.g., by the SSD, a thus *magnetically* driven SC dynamo exists (Squire & Bhattacharjee 2015, 2016). These studies reported the generation of a large-scale magnetic field, usually on the scale of the computational domain, with magnetic forcing while in the case of kinetic forcing only, the generated patterns were reported to be temporally more erratic and spatially less coherent. For a flow in y direction, sheared in x, an attempt was made to measure the turbulent transport coefficients using the Second Order Cumulant Expansion method of Marston et al. (2008), and the results indicated negative η_{yx} and η_{xx} in the presence of magnetic forcing. Incidentally, if confirmed in this case, a negative η_{xx} could also imply dynamo action (Lanotte et al. 1999; Devlen et al. 2013). At that time, however, a suitable test-field method (TFM), providing another measurement tool for the turbulent transport coefficients, was not yet available.

Here, we present first steps towards such a toolbox, extending the method developed by (Rheinhardt & Brandenburg 2010, (RB10)) to include the self–advection term and rotation, albeit still limited to simplified MHD (SMHD) equations, with the pressure gradient term being dropped. Although this method does not yet provide a completely suitable tool for the systems studied by Squire & Bhattacharjee (2015, 2016), it does provide a working solution for simplified shear dynamos with magnetic forcing, mimicking SSD, and can be envisioned to enable important scientific insights. In this paper, we present the method, referred to as "nonlinear test-field method" (NLTFM), and tests against previously studied cases, along with other validation results. As our major topic, we analyze runs with simplified MHD equations that exhibit dynamo action in the same parameter regime as previously claimed to host magnetic SC (MSC) effect dynamos.

2. MODEL AND METHODS

We perform local Cartesian box simulations with shearing-periodic boundary conditions to implement large-scale shear as a linear background flow imposed on the system. The shear occurs in the x direction, which could represent, e.g., the direction from the rotational centre of a cosmic body. Here, y is the stream-wise, or azimuthal, direction, and z points into the vertical direction. The magnitude of the shearing motion is described by the input parameter S such that the imposed linear shear flow is $\boldsymbol{U}^{\rm S} = Sx\hat{\boldsymbol{y}}$. The rotation of the domain, $\boldsymbol{\Omega} = (0,0,\Omega)$, is described by the input parameter Ω, the magnitude of the angular velocity. In most of the simulations reported in this paper, however, rotation is neglected, as here we concentrate on studying the possibility of the SC effect alone. We will, however, retain rotation in the model equations for completeness. Our boxes have edge lengths $L_x = L_y$, and L_z with aspect ratio $\mathcal{A} = L_z/L_x$ chosen $\mathcal{A} = 1$ in many cases, but we consider also vertically elongated boxes with $\mathcal{A} = 4, 8, 16$. All calculations were carried out with the PENCIL CODE.[1]

2.1. *Simplified MHD*

As stated in the introduction, the equations of SMHD as defined here are similar to those of MHD, but lack the pressure gradient. Correspondingly, the density ρ is held constant. We solve the equations for the magnetic vector potential $\boldsymbol{A}$ and the velocity $\boldsymbol{U}$,

$$\mathcal{D}^A\boldsymbol{A} = \boldsymbol{U}\times\boldsymbol{B} + \boldsymbol{F}_{\rm K} + \eta\boldsymbol{\nabla}^2\boldsymbol{A}, \tag{1}$$

$$\begin{aligned}\mathcal{D}^U\boldsymbol{U} = &-\boldsymbol{U}\cdot\boldsymbol{\nabla}\boldsymbol{U} + \boldsymbol{J}\times\boldsymbol{B}/\rho + \boldsymbol{F}_{\rm M}\\ &+\nu(\boldsymbol{\nabla}^2\boldsymbol{U} + \boldsymbol{\nabla}\boldsymbol{\nabla}\cdot\boldsymbol{U}/3)\end{aligned} \tag{2}$$

with the linear expressions

$$\mathcal{D}^A\boldsymbol{A} = \mathcal{D}\boldsymbol{A} + S\hat{\boldsymbol{x}}A_y, \tag{3}$$

$$\mathcal{D}^U\boldsymbol{U} = (\mathcal{D} + 2\boldsymbol{\Omega}\times)\boldsymbol{U} + S\hat{\boldsymbol{y}}U_x \tag{4}$$

$$\mathcal{D} = \partial/\partial t + Sx\partial/\partial y. \tag{5}$$

$\boldsymbol{B} = \boldsymbol{\nabla}\times\boldsymbol{A}$ is the magnetic field, $\boldsymbol{J} = \boldsymbol{\nabla}\times\boldsymbol{B}$ is the current density in units where the vacuum permeability is unity, $\boldsymbol{F}_{\rm K}$

---

[1] http://github.com/pencil-code

and $\boldsymbol{F}_{\rm M}$ are kinetic and magnetic forcing functions, respectively, η is the (molecular) magnetic diffusivity, and ν is the kinematic viscosity, both considered constant. Equation (2) can be considered a 3-dimensional generalization of Burgers' equation, which is why we refer to its turbulent solutions as "burgulence".

The main advantage of using SMHD is to avoid the necessity of dealing with density fluctuations and corresponding effects in the mean quantities. However, as self-advection $\boldsymbol{U}\cdot\boldsymbol{\nabla}\boldsymbol{U}$ is no longer discarded, we are here more general than RB10 the models of which suffered, in physical terms, from the implied assumption of slow fluid motions, that is, small Strouhal numbers (St $\ll 1$) or small Reynolds numbers (Re $\ll 1$). A complete neglect of the self-advection term is inadequate in the present context given that shear plays its essential role just via this term. So merely the terms arising from an additional mean flow and from the fluctuating velocity alone could be neglected. The latter neglect, however, would be equivalent to restricting the method to the second-order correlation approximation (SOCA) w.r.t. to the self-advection term which is not desirable.

2.2. *Full MHD*

The full MHD system of equations (FMHD), here with an isothermal equation of state, is more complex because of the occurrence of the pressure gradient, by which we need an additional evolution equation for the density. Also the viscous force is more complex, hence

$$\begin{aligned}\mathcal{D}^A\boldsymbol{A} &= \boldsymbol{U}\times\boldsymbol{B}+\boldsymbol{F}_{\rm K}+\eta\boldsymbol{\nabla}^2\boldsymbol{A},\\ \rho(\mathcal{D}^U+\boldsymbol{U}\cdot\boldsymbol{\nabla})\boldsymbol{U}+\boldsymbol{\nabla}p &= \boldsymbol{J}\times\boldsymbol{B}+\rho\boldsymbol{F}_{\rm M}+\boldsymbol{\nabla}\cdot(2\nu\rho\mathsf{S}),\\ (\mathcal{D}+\boldsymbol{U}\cdot\boldsymbol{\nabla})\ln\rho &= -\boldsymbol{\nabla}\cdot\boldsymbol{U}.\end{aligned}\qquad(6)$$

Here, $\mathsf{S}_{ij}=(U_{i,j}+U_{j,i})-\frac{1}{3}\boldsymbol{\nabla}\cdot\boldsymbol{U}$ are the components of the rate-of-strain tensor S, where commas denote partial differentiation, and p is the pressure related to the density via $p=c_{\rm s}^2\rho$, with $c_{\rm s}=\text{const}$ being the isothermal sound speed.

2.3. *Nonlinear TFM*

Throughout, we define mean quantities by horizontal averaging, i.e., averaging over x and y, denoted by an overbar. So they depend on z and t only. Fluctuations are denoted by lowercase symbols or a prime, e.g., $\boldsymbol{a}=\boldsymbol{A}-\overline{\boldsymbol{A}}$, $\boldsymbol{u}=\boldsymbol{U}-\overline{\boldsymbol{U}}$, and $(\boldsymbol{u}\times\boldsymbol{b})'=\boldsymbol{u}\times\boldsymbol{b}-\overline{\boldsymbol{u}\times\boldsymbol{b}}$. Normally taken to be a Reynolds average, in situations with shear the complication arises that $\overline{\boldsymbol{U}^S}\neq\boldsymbol{U}^S$ (when defined to be $\propto x$, the mean even vanishes), being hence not a pure mean, while $\partial_i U_j^S$ is spatially constant, hence a pure mean. However, $(\boldsymbol{U}^S\cdot\boldsymbol{\nabla}G)'=\boldsymbol{U}^S\cdot\boldsymbol{\nabla}g$ for an arbitrary quantity $G=\overline{G}+g$. This is a consequence of $\boldsymbol{U}^S\cdot\boldsymbol{\nabla}\overline{G}=0$ and $\overline{\boldsymbol{U}^S\cdot\boldsymbol{\nabla}g}=\int\!\!\int Sx\,\partial_y g\,dxdy=\int Sx\left(\int\partial_y g\,dy\right)dx=0$, the latter because of periodicity in y.

The evolution equations for the fluctuations of the magnetic vector potential, $\boldsymbol{a}$, and the velocity, $\boldsymbol{u}$, are following from Eqs. (1) and (2) as

$$\mathcal{D}^A\boldsymbol{a}=\boldsymbol{u}\times\overline{\boldsymbol{B}}+(\boldsymbol{u}\times\boldsymbol{b})'+\boldsymbol{f}_{\rm K}+\eta\boldsymbol{\nabla}^2\boldsymbol{a},\qquad(7)$$

$$\begin{aligned}\mathcal{D}^U\boldsymbol{u}=&\left(\overline{\boldsymbol{J}}\times\boldsymbol{b}+\boldsymbol{j}\times\overline{\boldsymbol{B}}+(\boldsymbol{j}\times\boldsymbol{b})'\right)/\rho+\boldsymbol{f}_{\rm M}\\ &+(\boldsymbol{u}\cdot\boldsymbol{\nabla}\boldsymbol{u})'+\nu\left(\boldsymbol{\nabla}^2\boldsymbol{u}+\boldsymbol{\nabla}\boldsymbol{\nabla}\cdot\boldsymbol{u}/3\right),\end{aligned}\qquad(8)$$

Terms with the mean flow $\overline{\boldsymbol{U}}$ have been dropped because they are suppressed in the simulations. Further, $\overline{\boldsymbol{F}}_{\rm K}=\overline{\boldsymbol{F}}_{\rm M}=\boldsymbol{0}$, that is, the forcings are pure fluctuations.

We solve these equations not by setting $\overline{\boldsymbol{B}}$ to the actual mean field resulting from the solutions of Eqs. (1) and (2), but by setting it to one of several test fields, $\boldsymbol{B}^{\rm T}$. Those are

$$\boldsymbol{B}^{(1)}=(\cos k_Bz,0,0),\quad\boldsymbol{B}^{(2)}=(\sin k_Bz,0,0),\qquad(9)$$

$$\boldsymbol{B}^{(3)}=(0,\cos k_Bz,0),\quad\boldsymbol{B}^{(4)}=(0,\sin k_Bz,0),\qquad(10)$$

where k_B is the wavenumber of the test field, being a multiple of $2\pi/L_z$. From the solutions of Eqs. (7) and (8) we can construct the mean electromotive force, $\overline{\boldsymbol{\mathcal{E}}}=\overline{\boldsymbol{u}\times\boldsymbol{b}}$ and the mean ponderomotive force, $\overline{\boldsymbol{\mathcal{F}}}=\overline{\boldsymbol{j}\times\boldsymbol{b}/\rho-\boldsymbol{u}\cdot\boldsymbol{\nabla}\boldsymbol{u}}$, which are then expressed in terms of the mean field by the ansatzes

$$\overline{\mathcal{E}}_i=\alpha_{ij}\overline{B}_j-\eta_{ij}\overline{J}_j,\qquad(11)$$

$$\overline{\mathcal{F}}_i=\phi_{ij}\overline{B}_j-\psi_{ij}\overline{J}_j,\qquad(12)$$

where i,j adopt only the values $1,2$ as a consequence of setting the anyway constant $\overline{B}_z$ arbitrarily to zero. Hence, each of the four tensors, α_{ij}, η_{ij}, ϕ_{ij}, ψ_{ij}, has four components, i.e., altogether we have 16 unknowns.

In the quasi-kinematic test-field method (QKTFM) (see Sect. 2.4), $\overline{\boldsymbol{\mathcal{E}}}$, considered as a functional of $\boldsymbol{u}$, $\overline{\boldsymbol{U}}$, and $\overline{\boldsymbol{B}}$, is linear in $\overline{\boldsymbol{B}}$. In the more general case with a magnetic background turbulence, this is a priori no longer the case. To deal with this difficulty, RB10 added the evolution equations for the background turbulence ($\boldsymbol{u}_0$,$\boldsymbol{b}_0$) which are similar to Eqs. (7) and (8), but for zero mean field, to the equations of the TFM. In general, $\overline{\boldsymbol{\mathcal{E}}}$ can be split into a contribution $\overline{\boldsymbol{u}_0\times\boldsymbol{b}_0}$ that is independent of the mean field and a contribution

$$\overline{\boldsymbol{\mathcal{E}}}_{\overline{\boldsymbol{B}}}=\overline{\boldsymbol{u}_0\times\boldsymbol{b}_{\overline{\boldsymbol{B}}}}+\overline{\boldsymbol{u}_{\overline{\boldsymbol{B}}}\times\boldsymbol{b}_0}+\overline{\boldsymbol{u}_{\overline{\boldsymbol{B}}}\times\boldsymbol{b}_{\overline{\boldsymbol{B}}}},\qquad(13)$$

where $\boldsymbol{u}_{\overline{\boldsymbol{B}}}$ and $\boldsymbol{b}_{\overline{\boldsymbol{B}}}$ denote the solutions of Eqs. (7) and (8) in the absence of any forcing (called "test problems") which are supposed to vanish for vanishing $\overline{\boldsymbol{B}}$. Using $\boldsymbol{u}=\boldsymbol{u}_0+\boldsymbol{u}_{\overline{\boldsymbol{B}}}$ and $\boldsymbol{b}=\boldsymbol{b}_0+\boldsymbol{b}_{\overline{\boldsymbol{B}}}$, $\overline{\boldsymbol{\mathcal{E}}}_{\overline{\boldsymbol{B}}}$ can be written in two equivalent ways as

$$\overline{\boldsymbol{\mathcal{E}}}_{\overline{\boldsymbol{B}}}=\overline{\boldsymbol{u}\times\boldsymbol{b}_{\overline{\boldsymbol{B}}}}+\overline{\boldsymbol{u}_{\overline{\boldsymbol{B}}}\times\boldsymbol{b}_0}=\overline{\boldsymbol{u}_0\times\boldsymbol{b}_{\overline{\boldsymbol{B}}}}+\overline{\boldsymbol{u}_{\overline{\boldsymbol{B}}}\times\boldsymbol{b}}.\qquad(14)$$

Both become linear in quantities with subscript $\overline{\boldsymbol{B}}$ when $\boldsymbol{b}$ and $\boldsymbol{u}$ are identified with the fluctuating fields in the main run, which is the system (1)–(2) solved simultaneously with the test solutions. In this way, we have recovered the mentioned linearity property of $\overline{\boldsymbol{\mathcal{E}}}[\overline{\boldsymbol{B}}]$ of the QKTFM. Likewise, one writes the part of the mean ponderomotive force $\overline{\boldsymbol{\mathcal{F}}}$, which results from the Lorentz force as

$$\overline{\boldsymbol{j}\times\boldsymbol{b}_{\overline{B}}}+\overline{\boldsymbol{j}_{\overline{B}}\times\boldsymbol{b}_0} \quad\text{or}\quad \overline{\boldsymbol{j}_0\times\boldsymbol{b}_{\overline{B}}}+\overline{\boldsymbol{j}_{\overline{B}}\times\boldsymbol{b}}\,; \qquad (15)$$

and that resulting from self-advection as

$$\overline{\boldsymbol{u}\cdot\boldsymbol{\nabla}\boldsymbol{u}_{\overline{B}}}+\overline{\boldsymbol{u}_{\overline{B}}\cdot\boldsymbol{\nabla}\boldsymbol{u}_0} \quad\text{or}\quad \overline{\boldsymbol{u}_0\cdot\boldsymbol{\nabla}\boldsymbol{u}_{\overline{B}}}+\overline{\boldsymbol{u}_{\overline{B}}\cdot\boldsymbol{\nabla}\boldsymbol{u}}\,; \quad (16)$$

see Equations (29) and (30) of RB10. Corresponding expressions can be established for the fluctuating parts of the bilinear terms, $(\boldsymbol{u}\times\boldsymbol{b})'$, $(\boldsymbol{j}\times\boldsymbol{b})'$, and $(\boldsymbol{u}\cdot\boldsymbol{\nabla}\boldsymbol{u})'$. We recall that the different formulations of the fluctuating parts, result in different stability properties of the test problems, see also the test results presented in Appendix B.1. Here we chose to use in Eqs. (14)–(16) and the corresponding versions of the fluctuating terms the first one, resulting in what is called the ju method; see Table 1 of Rheinhardt & Brandenburg (2010).

The kinematic limit—The given alternative formulations become equivalent when the mean quantities, possibly evolving in the main run, are too weak to have a marked influence on the fluctuating fields. Then, $\boldsymbol{u}\to\boldsymbol{u}_0$ and $\boldsymbol{b}\to\boldsymbol{b}_0$. Employing this means dropping terms like $\overline{\boldsymbol{u}_{\overline{B}}\times\boldsymbol{b}_{\overline{B}}}$ in mean EMF and mean force as is the correct way to obtain the latter as quantities of first order in $\overline{\boldsymbol{B}}$. Then all possible versions of the NLTFM (which actually ceases to be nonlinear) give identical results up to roundoff errors.

2.4. *Quasikinematic TFM*

We now state here for comparison the governing equations for the QKTFM (see also Schrinner et al. 2005, 2007). They consist of just Eq. (7), but not Eq. (8), and Eq. (11). Then, Eq. (14) reduces simply to

$$\overline{\boldsymbol{\mathcal{E}}}_{\overline{B}} = \overline{\boldsymbol{u}\times\boldsymbol{b}_{\overline{B}}} \qquad (17)$$

Obviously, the contribution $\overline{\boldsymbol{u}_{\overline{B}}\times\boldsymbol{b}_0}$ is missing. Again, for further details see RB10.

2.5. *Forcing*

The standard forcing, implemented in the PENCIL CODE, employs white–in–time “frozen” harmonic non-helical plane waves. Their wavevectors are randomly selected from a thin shell in k space of radius k_f that fit into the periodic computational domain (for details see, e.g. Käpylä et al. 2020). In most of our simulations, we apply this forcing for both $\boldsymbol{f}_\mathrm{K}$ and $\boldsymbol{f}_\mathrm{M}$ in Eqs. (7) and (8). The wavevectors are further selected such that no mean field or mean flow are directly sustained, that is, the case $k_y = 0$ is excluded.[2] However, due to roundoff errors, it is unavoidable that averages over harmonic functions deviate slightly from zero. We call this effect “leakage of the forcing into the mean fields”. Being without effect for the velocity as we remove its mean permanently, strong shear could produce a linearly growing $\overline{B}_y$ out of a small $\overline{B}_x$ due to such leakage. This is why we checked its effect in purely magnetic runs and found the growth of $\overline{B}_y$ to be limited and both components to stay within margins close to numerical precision. Nevertheless, as will be discussed in Sect. 3.1, with this magnetic forcing setup, the mean magnetic fields very quickly (in a few turnover times) reach dynamically effective strengths without showing a clear exponential stage.

Hence, another forcing setup was designed, referred to as “decimated forcing”. In addition to ensuring that the case $k_y = 0$ is excluded, we took out all those wavevectors for which $|k_{x,y,z}|/k_1 \leq k_\mathrm{min}/k_1 = 2$. As will be discussed in the results section, the decimated forcing has the advantage of reducing the amplitude of the mean fields generated during the initial stages, thus allowing us to determine the growth rate of an exponentially growing dynamo instability. While the standard choice is expected to provide a good approximation to homogeneous isotropic velocity turbulence, isotropy could be lost in the decimated case, given that all wavevectors are parallel or almost parallel to the spatial diagonals of the box.

However, as is discussed in Appendix A, the generated turbulence does not markedly deviate from that by the standard forcing in terms of isotropy. Also, repeating the kinetically forced runs ($\boldsymbol{f}_\mathrm{M} = \boldsymbol{0}$) with decimated forcing do not significantly alter the dynamo solutions.

2.6. *Input and output quantities*

The simulations are fully defined by choosing the shear parameter S, the forcing setup, amplitude, and wavenumber, k_f, the kinematic viscosity ν, and the magnetic diffusivity η. The boundary conditions are (shearing) periodic in all three directions. The following quantities are used as diagnostics: We quantify the strength of the turbulence by the fluid and magnetic Reynolds numbers

$$\mathrm{Re} = \frac{u_\mathrm{rms}}{\nu k_\mathrm{f}}, \quad \mathrm{Re}_\mathrm{M} = \frac{u_\mathrm{rms}}{\eta k_\mathrm{f}} = \mathrm{Pr}_\mathrm{M}\,\mathrm{Re}, \qquad (18)$$

where

$$\mathrm{Pr}_\mathrm{M} = \frac{\nu}{\eta}, \qquad (19)$$

is the magnetic Prandtl number, along with the Lundquist number,

$$\mathrm{Lu} = \frac{B_\mathrm{rms}}{\eta k_\mathrm{f}}. \qquad (20)$$

The strength of the imposed shear is measured by the dynamic shear number

$$\mathrm{Sh}_\mathrm{K} = \frac{S}{u_\mathrm{rms} k_\mathrm{f}}. \qquad (21)$$

---

[2] Without shear, only those with $k_x = k_y = 0$ had to be excluded, but due to shear-periodicity, $2\pi/k_x$ is no longer an integer fraction of L_x.

As in earlier work, we normalize the turbulent magnetic diffusivity tensor by the SOCA estimate

$$\eta_0 = u_{\rm rms}/3k_{\rm f} \qquad (22)$$

or the molecular diffusivity η. The magnetic field is normalized by the equipartition field strength, $B_{\rm eq} = \langle \mu_0 \rho \boldsymbol{u}^2 \rangle^{1/2}$, where μ_0 is the vacuum permeability (here set equal to unity) and angle brackets denote volume averaging.

We define the root-mean-square (rms) value of a field $\boldsymbol{V}$ as $V_{\rm rms} = \langle \boldsymbol{V}^2 \rangle^{1/2}$. The rms values of the mean field components are computed as $\overline{B}_{i,\rm rms} = \langle \overline{B}_i^2 \rangle_z^{1/2}$, where $\langle . \rangle_z$ denotes averaging over z.

2.7. *Resetting*

The test problems Eqs. (7) and (8) are often unstable, but this does not necessarily affect the values of the resulting turbulent transport coefficients: They usually show statistically stationary behavior over limited time spans although the test solutions are already growing. For safety reasons, we always reset them to zero in regular intervals (typically every 50 time units); see Hubbard et al. (2009) for a discussion. We also remove 20% of data from the beginning of each resetting interval, to mask the initial transient due to the resetting.

2.8. *Mean flow removal*

In all cases, be it full or simplified MHD, the first instability to be excited is the generation of mean flows in the horizontal velocity components. These are most likely signatures of the vorticity dynamo (see, e.g., Elperin et al. 2003; Käpylä et al. 2009). They have a strong effect on the dynamics and can de-stabilize the test problems. Therefore, we have decided to suppress all mean flows by subtracting them from the solution $\boldsymbol{U}$ in every timestep. We will return to their effect in a forthcoming publication.

3. RESULTS

The naming of the runs is such that the first letter, F or S, indicates full or simplified MHD, while the second and/or third refers to the forcing regime: K and KM referring to purely kinetic and combined kinetic and magnetic forcing with equal amplitude, respectively. The number following the letters indicates the vertical aspect ratio $\mathcal{A}$ of the box. A trailing letter “d” stands for “decimated forcing”.

3.1. *Overall behavior of the main runs*

As our starting point, we defined a setup, related to one from Squire & Bhattacharjee (2015), with marginal dynamo excitation (in incompressible MHD) with an aspect ratio $\mathcal{A} = 8$. We denote this run as FK8a, and tabulate ${\rm Re}_{\rm M}$, the growth rate of the initial kinematic stage, λ, and the $\boldsymbol{\eta}$ components measured by QKTFM in Table 1. As reported by Squire & Bhattacharjee (2015), we also observe an initial decay of the rms and mean magnetic fields, but later on temporary saturation at very low values, after which a very slow decay is observed, indicative of a nearly marginally excited dynamo state. Due to the finite $\overline{B}_x$ present at all times, a much stronger (roughly 40 times) $\overline{B}_y$ is maintained due to the shear, but as the dynamo is nearly marginal, these mean fields remain at very low strengths.

Next, we repeat this run, but with SMHD which yields Run SK8a in Table 1. Now rms and mean fields grow, the mean radial and azimuthal components showing exponential growth at the same rate, albeit still very slow. Nevertheless, the dynamo instability is somewhat easier to excite than in FMHD. The azimuthal component is again much stronger than the radial one with the ratio $\overline{B}_{y,\rm rms}/\overline{B}_{x,\rm rms}$ similar to the FMHD case.

We continue by repeating these runs with decreased magnetic diffusivity, resulting in roughly six times larger magnetic Reynolds number, ${\rm Re}_{\rm M}$ (Runs FK8b and SK8b). In both simulations we observe exponential growth of the rms and mean magnetic fields, somewhat faster with SMHD than with FMHD. We also determine the fastest growing dynamo mode and its vertical wavenumber, k_z and list them in Table 3; the fastest growing mode is the nearly the same, $k_z/k_1 = 9$, in both models. Hence, we can conclude that, going from FMHD to SMHD retains the dynamo mode, but changes its excitation condition and growth rate somewhat.

As the dynamo growth is slow, simulations with $\mathcal{A} = 8$ are too costly to be run until saturation. Hence, to investigate whether with reduced $\mathcal{A}$ the dynamo mode could be retained, we repeated the runs with $\mathcal{A} = 1$ (Runs FK1a, FK1b, SK1a and SK1b). As is evident from Tables 1 and 3, these runs behave very much like their tall box counterparts, the low-${\rm Re}_{\rm M}$ FMHD model being slightly subcritical and the high-${\rm Re}_{\rm M}$ one supercritical, while the SMHD runs are both supercritical. The fastest growing mode now has $k/k_1 = 1$, corresponding to $k/k_1 = 8$ in the tall box. We also perform a set of runs in SMHD with $\mathcal{A} = 4$; see Runs SK4a and SK4b. The former exhibits a very slowly decaying solution instead of a growing one, which is an anomaly in the SMHD set, but the latter one, again, exhibits a growth rate very similar to the cubic (SK1b) and tall box (SK8b) cases, both with a wavenumber $k_z/k_1 = 4$. All in all, the ‘b’ runs give rather clear evidence that the cubic simulation domains retain the same dynamo mode as the taller ones.

The time evolution of the rms and mean fields from the cubic runs, integrated until saturation, are shown in the top panel of Figure 1 with solid and broken lines, respectively. The growth rate of the SMHD run is somewhat larger, but the saturation strength is lower than in FMHD. The ratio $\overline{B}_{y,\rm rms}/\overline{B}_{x,\rm rms}$, however, is the same. We also show the mean fields in a zt diagram in Figure 2, top panel. We see the emergence and saturation of the Fourier mode $k = 1$ both in the radial and azimuthal components, where each negative (positive) patch of $\overline{B}_y$ is accompanied by a much weaker positive

Table 1. Summary of the runs with constant shear and forcing wavenumber.

Run	$\mathrm{Re_M}$	$\lambda/(\eta_0 k_\mathrm{f}^2)$	η_{xx}/η_0	η_{yy}/η_0	η_{yx}/η_0	η_{xy}/η_0	$\alpha_\mathrm{rms}/\eta_0 k_\mathrm{f}$	η_rms/η_0
FK1a	2.1	−0.0354	0.557±0.006	0.547±0.007	0.048±0.001	0.351±0.009	0.018±0.009	0.054±0.013
FK1b	11.9	0.0140	0.608±0.015	0.598±0.014	0.023±0.001	0.419±0.032	0.022±0.011	0.031±0.012
FK8a	2.1	−0.0008	0.572±0.010	0.563±0.011	0.044±0.002	0.378±0.009	0.001±0.002	0.048±0.014
FK8b	12.7	0.0166	0.641±0.019	0.634±0.017	0.023±0.001	0.473±0.024	0.009±0.005	0.026±0.009
SK1a	2.0	0.0006	0.367±0.001	0.393±0.002	−0.003±0.000	0.279±0.002	0.021±0.004	0.009±0.001
SK1b	12.3	0.0183	0.440±0.004	0.412±0.001	−0.011±0.002	0.461±0.009	0.020±0.009	0.017±0.009
SK4a	2.1	−0.0042	0.367±0.003	0.390±0.003	−0.004±0.000	0.279±0.003	0.008±0.002	0.006±0.001
SK4b	13.3	0.0185	0.334±0.037	0.339±0.044	−0.004±0.005	0.239±0.073	0.008±0.004	0.007±0.008
SK8a	2.1	0.0033	0.367±0.003	0.390±0.004	−0.003±0.000	0.274±0.003	0.006±0.002	0.005±0.002
SK8b	12.8	0.0192	0.401±0.005	0.424±0.005	−0.015±0.000	0.367±0.010	0.007±0.002	0.017±0.004
SKM1a	1.9	—	1.794±0.039	1.278±0.045	0.200±0.025	−0.725±0.083	0.010±0.055	0.250±0.090
SKM4a	2.1	—	2.012±0.179	1.191±0.014	0.221±0.012	−0.560±0.015	0.046±0.017	0.230±0.072
SKM8a	1.8	—	3.054±0.625	1.481±0.131	0.338±0.064	−0.186±0.045	0.036±0.011	0.352±0.213
SKM16a	2.0	—	2.238±0.552	1.215±0.010	0.249±0.062	−0.580±0.055	0.022±0.008	0.260±0.191
SKM1ad	2.1	0.0103	1.228±0.214	1.326±0.074	0.247±0.043	0.237±0.117	0.149±0.062	0.441±0.212
SKM4ad	1.9	0.0315	1.279±0.150	1.455±0.066	0.222±0.022	0.369±0.072	0.081±0.017	0.270±0.119
SKM8ad	1.5	0.0948	1.688±0.165	2.040±0.150	0.516±0.061	0.383±0.154	0.111±0.069	0.543±0.260

Notes: For all runs, $k_\mathrm{f}/k_1 = 5$ ($k_1 = 2\pi/L_x$), and $S = -0.25$, yielding a roughly invariable $\mathrm{Sh_K}$ of -1.6. In runs with labels 'a', the magnetic Prandtl number $\mathrm{Pr_M}$ is $1/3$, while for 'b' it is 20.

(negative) patch in $\overline{B}_x$. The patches disappear and re-appear quasi-periodically, and also their vertical position is not constant. In comparison to Squire & Bhattacharjee (2015), who show similar plots of simulations with parameters closely matching ours, the appearance of $\overline{B}_y$ in their purely kinetically forced run (their Figure 9(a)) is much more erratic than in our SMHD runs. Comparing to the kinetically forced FMHD results of Brandenburg et al. (2008) (their Figure 7), however, our solution looks very similar, although they had much higher $\mathrm{Re_M}$ and also higher $\mathrm{Pr_M}$, which should have enabled a simultaneous SSD.

Finally, we repeat the simulations, labelled 'a' ($\mathrm{Pr_M} = 1/3$), with the same parameters, but using the magnetic forcing in addition to the kinetic one, so that the same rms velocity is obtained as in the kinetically forced cases, with equal contributions from the kinetic and magnetic forcings. This set of parameters should very closely correspond to the case studied in Squire & Bhattacharjee (2015), Figure 9(d). As seen there, too, we observe a nearly immediate appearance (during the first five turnover times) of a strong $\overline{B}_y$ as is shown for Run SKM1a in Figure 1, lower panel. Although Squire & Bhattacharjee (2015) did not show the evolution of $\overline{B}_x$, our results give indication that $\overline{B}_y$ arises due to the action of the strong shear on $\overline{B}_x$. After the initial rapid growth, we do not see any further increase of $\overline{B}_x$ while linear growth up to $tu_\mathrm{rms}k_\mathrm{f} \approx 170$ and quasi-regular oscillations occur in $\overline{B}_y$. Hence, we are not able to report a growth rate for Run SKM1a in Table 1, and also not for the larger $\mathcal{A}$ runs SKM4a, SKM8a and SKM16a for the same reason. From Figure 2, middle panel, we see that, again, the $k_z = 1$ vertical Fourier mode is the preferentially excited one, although the patterns seen in the zt plots are much more short–lived and erratic in time than in the kinetically forced counterpart SK1a (same figure, top panel). Remarkably, there is no kinematic stage, but the large–scale pattern appears nearly instantly. (Note that the whole time range shown for Run SKM1a is roughly as long as the kinematic range exhibited by Run SK1b.) The appearance and evolution of $\overline{B}_y$ also disagrees with the results of Squire & Bhattacharjee (2015), who observed a much less erratic pattern to arise in a closely matching parameter regime see their Figure 9(d).

The rapidly emerging mean fields in the magnetically forced runs are related to the standard forcing scheme used in all the simulations presented so far. Even if this scenario could be regarded as a genuine dynamo instability, its investigation is out of the scope of our current numerical setup, because obviously much higher cadence in time should be used in an attempt to follow the possible kinematic stage. Also, the simulations should be started from a fully matured turbulent MHD background state, as currently the mean–field growth occurs during the initial transient state, where even turbulence itself is not yet saturated.

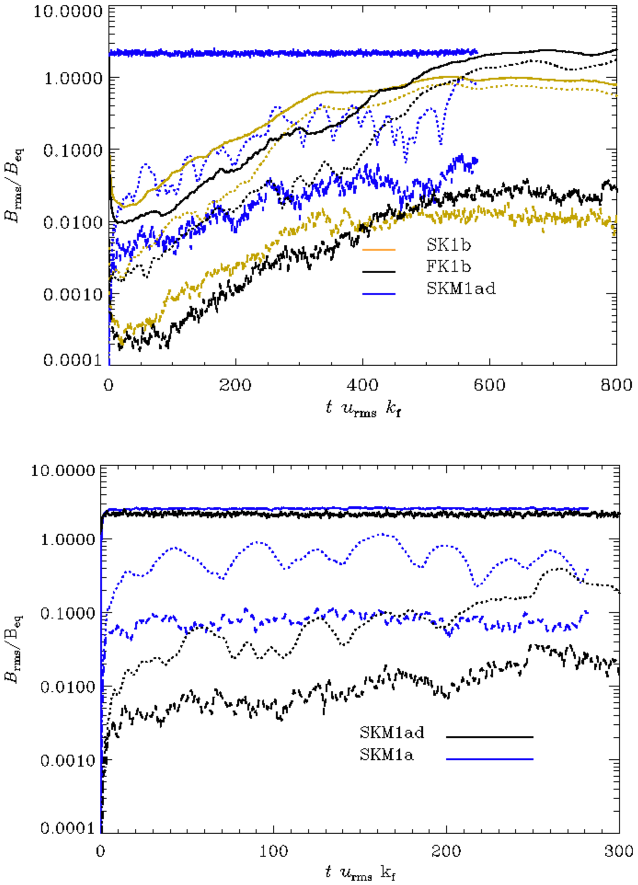

Figure 1. Time evolution of rms and mean magnetic field strengths from different runs. Top: comparison of a higher–Rm FK (black), an SK (orange), and a decimated SKM run (blue). Bottom: comparison of SKM runs with $\mathcal{A} = 1$, with standard (blue, Run SKM1a) and decimated (black, Run SKM1ad) forcing. Solid - $B_{\rm rms}$, dotted - $\overline{B}_{y,{\rm rms}}$, dashed - $\overline{B}_{x,{\rm rms}}$.

Hence, instead of fully dwelling on the cause of the rapid initial growth, we turn into using the decimated forcing function with $k_{\rm min} = 2$, and repeat Run SKM1a as a decimated version, now denoted SKM1ad and shown in Figure 1 lower panel (black lines). We still see the rapid appearance of the mean fields, but their magnitudes are now much lower than in the case of our standard forcing, plotted with blue lines in the same figure for comparison. After the rapid excitation phase, we observe a slow exponential growth of both $\overline{B}_x$ and $\overline{B}_y$, reminiscent of the dynamo instability seen in the FK and SK runs. The growth rate is now larger than in the kinetically forced counterparts FK1a and SK1a, see Table 1; when compared with the higher–$\rm Re_M$ runs FK1b and SK1b, as can be seen from Figure 1 upper panel, the growth rates are nearly equal. We also produced two more runs with varying aspect ratio $\mathcal{A}$ (SKM1ad and SKM8ad), and notice that the growth rate is increasing with $\mathcal{A}$.

Based on these runs with different forcings, we propose that the slow dynamo instability could have been drowned by the stronger initial mean fields when forced with the standard forcing function. Although the growth rate of the dynamo instability is similar to the kinetically forced cases, and the growing wavenumber of the dynamo instability are the same in both cases, the change of the growth rate as function of the aspect ratio of the box indicates that some key properties of the dynamo instability do change when magnetic forcing is used. In the next section we make an attempt to investigate what exactly has changed by measuring the turbulent transport coefficients in the systems with the relevant TFM variant.

3.2. *Turbulent transport coefficients*

3.2.1. *Strong shear cases*

In this subsection we compare cases of strong shear in kinetically forced FMHD and SMHD, and kinetically and magnetically forced SMHD, measured with the appropriate variant of the TFM. We choose $S = -0.25$, which, with the selected amplitude of the forcing, results in the shear number $\rm Sh_K \approx -1.6$, indicating a strong influence of shear on the system. This setup closely matches the cases investigated by Squire & Bhattacharjee (2015).

First we use the QKTFM to measure the turbulent transport coefficients in the kinetically forced FMHD cases, the results being presented in Table 1. We measure zero mean in all α components, hence we tabulate only the rms values of the α fluctuations; $\alpha_{\rm rms} = \langle\alpha_{ij}^2\rangle_t^{1/2}$. the same applies to all other runs studied here. In the low $\rm Re_M$ cases (FK1a, FK8a) we measure relatively isotropic diagonal components of the η tensor, positive and somewhat smaller values of η_{xy} and much smaller positive values of η_{yx}. The magnitude of the normalized η_{yx} values, however, exceeds the corresponding fluctuations in α. In these cases, no indications of LSD instability is seen.

In the high $\rm Re_M$ cases (FK1b and FK8b), the diagonal components of $\boldsymbol{\eta}$ have, as expected, higher magnitudes, showing only mild anisotropy, as in the low $\rm Re_M$ cases, so that the η_{xx} somewhat exceeds η_{yy}. η_{xy} is increased with respect to the diagonal components, reaching roughly 3/4 of their magnitudes. η_{yx} is still positive, and decreases in magnitude. In these cases we see LSD action, but with η_{yx} being positive, it seems unlikely that the dynamo is of SC-origin, in agreement with previous numerical studies (Yousef et al. 2008; Brandenburg et al. 2008; Singh & Jingade 2015). They did not consider as large values of the shear parameter as here, so we can now extend this conclusion to the strong shear regime. This is consistent with a series of earlier analytical works which treated shear non-perturbatively

Table 2. Summary of the runs with varying shear.

Run	$\mathrm{Sh_K}$	η_{xx}/η_0	η_{yy}/η_0	η_{yx}/η_0	η_{xy}/η_0	$\alpha_\mathrm{rms}/(\eta_0 k_\mathrm{f})$	η_rms/η_0
SKM1a001	-0.094	2.125 ± 0.028	2.129 ± 0.012	0.030 ± 0.016	0.001 ± 0.009	0.094 ± 0.015	0.137 ± 0.050
SKM1a002	-0.187	2.126 ± 0.024	2.131 ± 0.009	0.045 ± 0.009	-0.023 ± 0.003	0.101 ± 0.029	0.142 ± 0.066
SKM1a003	-0.278	2.120 ± 0.023	2.123 ± 0.015	0.061 ± 0.006	-0.035 ± 0.009	0.092 ± 0.034	0.137 ± 0.036
SKM1a004	-0.369	2.123 ± 0.011	2.121 ± 0.013	0.088 ± 0.005	-0.063 ± 0.017	0.096 ± 0.014	0.153 ± 0.043
SKM1a005	-0.458	2.122 ± 0.020	2.109 ± 0.013	0.093 ± 0.017	-0.084 ± 0.009	0.081 ± 0.033	0.147 ± 0.047
SKM1a006	-0.547	2.101 ± 0.013	2.074 ± 0.003	0.107 ± 0.017	-0.125 ± 0.005	0.088 ± 0.032	0.164 ± 0.071
SKM1a008	-0.719	2.084 ± 0.004	2.046 ± 0.023	0.133 ± 0.022	-0.173 ± 0.014	0.084 ± 0.019	0.173 ± 0.081
SKM1a009	-0.808	2.116 ± 0.048	2.049 ± 0.016	0.165 ± 0.013	-0.218 ± 0.024	0.077 ± 0.032	0.196 ± 0.074
SKM1a01	-0.873	2.057 ± 0.033	1.962 ± 0.016	0.164 ± 0.023	-0.237 ± 0.031	0.081 ± 0.034	0.196 ± 0.083
SKM1a011	-0.947	2.053 ± 0.037	1.932 ± 0.006	0.165 ± 0.008	-0.275 ± 0.019	0.080 ± 0.031	0.197 ± 0.073
SKM1a015	-1.226	1.968 ± 0.014	1.775 ± 0.027	0.193 ± 0.019	-0.391 ± 0.033	0.074 ± 0.027	0.219 ± 0.094
SKM1a02	-1.582	1.963 ± 0.070	1.622 ± 0.015	0.219 ± 0.010	-0.535 ± 0.007	0.067 ± 0.018	0.233 ± 0.068
SKM1a021	-1.623	1.911 ± 0.011	1.553 ± 0.008	0.220 ± 0.025	-0.542 ± 0.018	0.064 ± 0.030	0.238 ± 0.103
SKM1a025	-1.709	1.769 ± 0.026	1.303 ± 0.012	0.207 ± 0.018	-0.549 ± 0.055	0.058 ± 0.030	0.223 ± 0.083
SKM1a031	-1.985	1.676 ± 0.058	1.150 ± 0.011	0.228 ± 0.012	-0.628 ± 0.053	0.056 ± 0.024	0.238 ± 0.069
SKM1a0325	-2.057	1.662 ± 0.103	1.114 ± 0.024	0.224 ± 0.002	-0.663 ± 0.110	0.050 ± 0.014	0.236 ± 0.035
SKM1a035	-2.156	1.630 ± 0.062	1.060 ± 0.004	0.238 ± 0.013	-0.686 ± 0.023	0.052 ± 0.012	0.248 ± 0.083

Notes: Forcing wavenumber $k_\mathrm{f}/k_1 = 5$. The magnetic Reynolds number, $\mathrm{Re_M}$, varies from 1.4 (for weak shear) to 2.1 (for strong shear), and the Lundqvist number, Lu, from 4.2 (for weak shear) to 4.8 (for strong shear).

and found no evidence of SC-assisted LSD (Sridhar & Subramanian 2009a,b; Sridhar & Singh 2010; Singh & Sridhar 2011). We analyze the possible dynamo driving mechanism in more detail in Sect. 3.3.

Next we turn to the kinetically forced SMHD cases, analyzed both with the QKTFM and NLTFM, yielding consistent results, as discussed in Sect. B.2. The biggest difference to FMHD is that all η components are systematically smaller in SMHD, and moreover, η_{yx} has changed sign to negative values, being statistically significant within errors; see Table 1. Also, the rms α values are similar or a bit larger, and clearly exceed the η_{yx} component. In the face of the turbulent transport coefficients, it seems understandable that for the low $\mathrm{Re_M}$ cases the LSD is excited in SMHD, but not in FMHD, as the diffusive coefficients are lower, while the inductive ones are larger. Also, the sign of η_{yx} would now be favorable to enable the SC effect to support a LSD. Further, it is noteworthy that the diagonal components of $\boldsymbol{\eta}$ become more notably anisotropic, but now η_{yy} mostly exceeds η_{xx}. In Figure 3, we show for Run SK1b the probability density distributions of all tensor components. The diagonal $\boldsymbol{\alpha}$ components exhibit larger values than the off-diagonal ones, α_{xx} being especially strong. The off-diagonal components are very similar to each other, while α_{yy} is slightly larger than them, but clearly smaller than α_{xx}. The diagonal η components are close to being isotropic. η_{yx} is fluctuating tightly around zero, and exhibits a very small negative mean. The distribution of η_{xy} is broad, but always in the positive.

Lastly, we turn to the kinetically and magnetically forced SMHD cases, analyzed with the NLTFM. In the low-$\mathrm{Re_M}$ runs, all components of $\boldsymbol{\eta}$ show larger magnitudes in comparison to the kinetically forced cases. Its diagonal components now show very strong anisotropy, with η_{xx} being again dominant over η_{yy} as in the FMHD cases. η_{xy} has changed sign to negative values, while η_{yx} is again positive. The rms values of α and η are (mostly) increased, in particular those of the latter. The probability density functions of the transport coefficients, shown in Figure 3, right column, show clearly the anisotropy of the diagonal components of $\boldsymbol{\eta}$ and the sign change of η_{xy} to large negative values, with η_{yx} now exhibiting a clearly positive mean with some negative values as well. The α components are very similar to the kinetically forced SMHD case, with α_{xx} attaining much larger values than α_{yy} and the off-diagonal components. The positive sign of η_{yx} rules out the existence of a SC–effect dynamo in these cases. As will be discussed in detail in Sect. 3.3, the α and η fluctuations then remain as possible candidates to provide the necessary ingredients for a LSD.

3.2.2. *Dependence on the shear parameter*

In this section we report on the dependence of the turbulent transport coefficients on the shear number $\mathrm{Sh_K}$ in runs with both kinetic and magnetic forcing. We list our runs, their basic diagnostics, and the turbulent transport coefficients measured with the NLTFM, in Table 2. As the standard forcing was used here, we did not see any exponential growth in the evolution of the mean fields; see Sect. 3.1 for a rea-

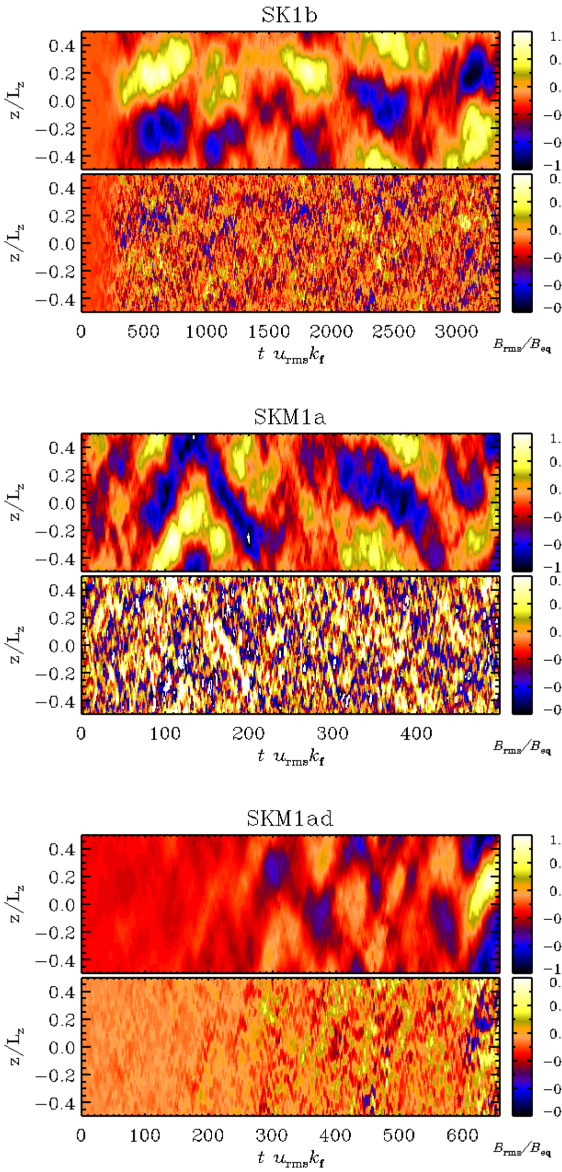

Figure 2. Butterfly (zt) diagrams of $\overline{B}_y$ (first, third and fifth panel) and $\overline{B}_x$ (second, fourth and sixth panel). Run SK1b is kinetically forced SMHD, SKM1a kinetically and magnetically forced SMHD, and SKM1ad is a counterpart of SKM1a, but with decimated forcing.

soning. Hence, no growth rates are reported, and we note that all the transport coefficients are measured from a stage, where the mean magnetic fields are dynamically significant. Our purpose is to scan a wider range of shear strengths for possible occurrences of a negative η_{yx} as function of Sh_K, which could enable an SC-driven LSD. The results are depicted in Figure 4, where we present the $\boldsymbol{\eta}$ components in two different normalizations. As can be seen, with weak shear ($|\mathrm{Sh}_\mathrm{K}| < 0.5$), the diagonal components of $\boldsymbol{\eta}$ are isotropic, while with stronger shear, anisotropy develops such that η_{xx} linearly increases while η_{yy} linearly decreases in the SOCA normalization. Normalizing to molecular diffusivity, both components are decreasing linearly, η_{xx} less steeply than η_{yy}. For weak shear, η_{yx} adopts small positive values, which keep increasing linearly with shear in the SOCA normalization. The linear trend is less clear in the molecular diffusivity normalization. Furthermore, η_{xy} attains weakly negative values for weak shear, and increasingly negative ones for strong shear. The trend is very close to linear when molecular diffusivity is used for normalization. Hence, we find no possibility for an MSC effect driven dynamo at any shear number investigated.

The dependencies of η_{ij} on shear, as obtained here, are in broad agreement with the results of Singh & Sridhar (2011) based on an analytical study in which arbitrarily large values of the shear parameter S could be explored; see references therein for more discussion. The two off-diagonal components η_{xy} and η_{yx} were found to start from zero at zero shear and, while the more relevant η_{yx} increases with $|S|$ to remain positive, η_{xy} behaves in a more complicated manner than found here, exhibiting both signs depending on the value of S: It decreases with increasing $|S|$ to become negative up to a certain value of shear, as in the present work; we refer the reader to Singh & Sridhar (2011) for more detail on its behavior at larger shear.

3.2.3. *Dependence on the aspect ratio*

We have studied the dependence of the turbulent transport coefficients on the aspect ratio $\mathcal{A}$ of the domain in the three different cases (FMHD, SMHD with kinetic/kinetic and magnetic forcing) with fixed shear parameter $S = -0.25$. The measured growth rate of the rms magnetic field, which coincides with the ones of of $\overline{B}_x$ and $\overline{B}_y$ except for standard magnetic forcing, and the measured turbulent transport coefficients are listed in Table 1; see runs with labels 4, 8, and 16, indicating $\mathcal{A}$.

In the kinetically forced FMHD and SMHD cases, the growth rate of the magnetic field is largely independent of the aspect ratio of the box, indicating that always one and the same dynamo mode is growing. We also measure the vertical wavenumber of the fastest growing dynamo mode in the kinematic stage, (see Table 3) which support this conclusion, as we see the wavenumber increasing proportional to $\mathcal{A}$. The turbulent transport coefficients do not show a marked dependence on $\mathcal{A}$ either.

In SMHD with standard kinetic and magnetic forcing, the situation is somewhat different. As we cannot draw conclusions on the growth rate of the magnetic field in these cases, we use the corresponding cases with decimated forcing as a

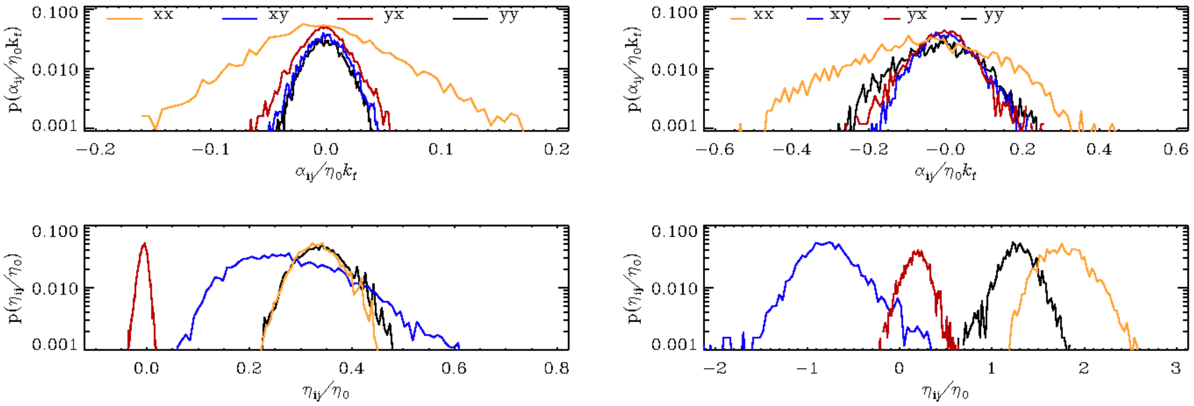

Figure 3. Probability density functions of all turbulent transport coefficients. Top: α_{ij}, bottom: η_{ij}. Left: kinetically forced SMHD Run SK1b, right: kinetically and magnetically forced SMHD Run SKM1a.

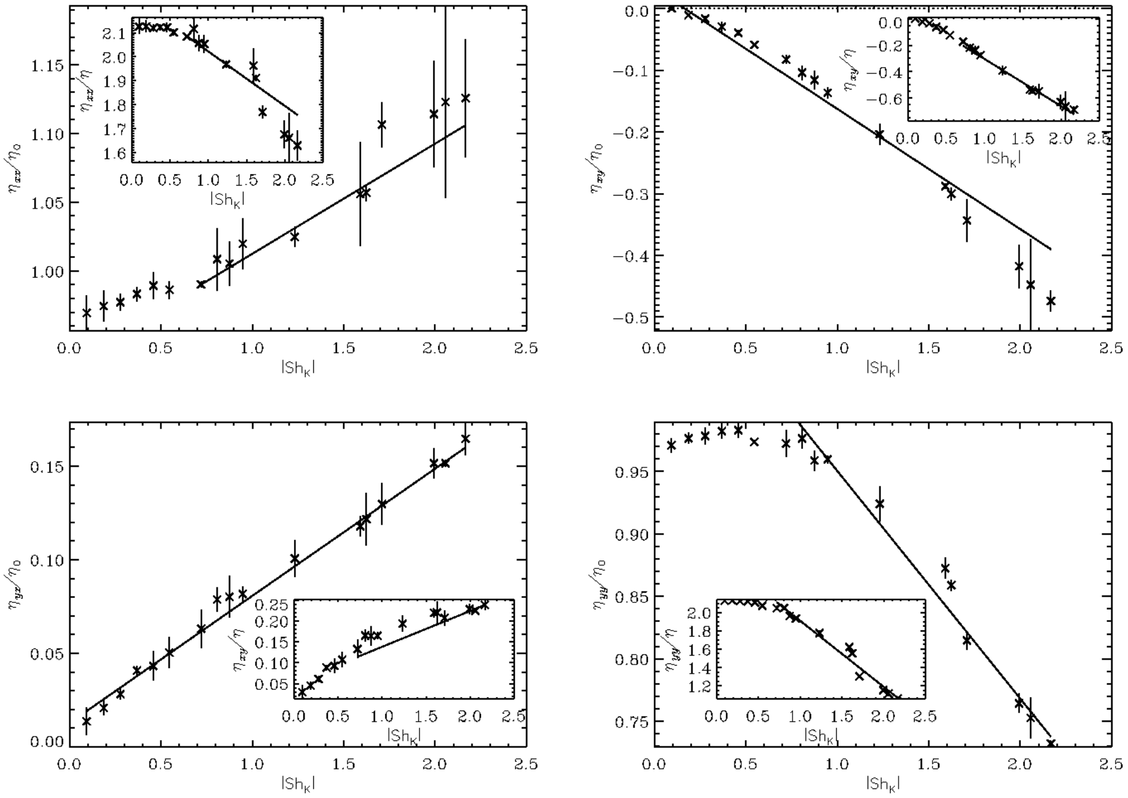

Figure 4. Dependence of the turbulent diffusivity tensor components, measured with NLTFM, on the shear number in the kinetically and magnetically forced cases. In the big plots we normalize to the SOCA estimate η_0, while in the insets to the molecular diffusivity η.

guideline. The latter (see Table 1, runs with label end ‘d’) show that the growth rate is increasing with $\mathcal{A}$, but we did not have the resources to verify this trend for the tallest box with $\mathcal{A} = 16$. In Figure 5 we show η_{yx} as a function of $\mathcal{A}$. It can be seen that the magnitudes of the turbulent transport coefficients change somewhat as function of the aspect ratio, although the magnitudes seem to saturate for the tallest box. The diagonal components grow in magnitude, η_{xx} somewhat more than η_{yy} making the anisotropy in the turbulent diffusivity even larger. The negative values measured for η_{xy} tend to get smaller in taller boxes. The positive values of η_{yx} increase with $\mathcal{A}$, hence we see no tendency for larger boxes to be more favorable for the SC dynamo. The fluctuating α and η behave similarly, with their magnitudes first increasing, but then decreasing for the tallest box. The decimated forcing cases show a similar trend for $\mathcal{A} = 4$ and 8 (SKM4ad and SKM8ad) while the case $\mathcal{A} = 1$ (SKM1ad) shows higher values of the transport coefficients not agreeing with this trend.

As the number of grid points is proportional to $\mathcal{A}$ at fixed resolution, resource limitations dictated to integrate the large $\mathcal{A}$ runs only over significantly shorter time spans. However, as we have discussed above, the mean fields grow initially very rapidly in all runs with standard forcing, irrespective of the aspect ratio. Hence, the effect of the different integration times on the values of transport coefficients can be ruled out.

One could also speculate that some spatio-temporal nonlocality (see e.g. Rheinhardt & Brandenburg 2012) might come into play with magnetic forcing, but when choosing our forcing wavenumbers, we have taken care of the $k_{\rm f}$ being scaled with respect to the computation domain vertical extent such that the forcing wavenumber should have remained constant. Our procedure, however, does not take into account memory effects in any way.

The dependence of the growth rate on the aspect ratio could also be due to different dynamo modes being excited in boxes of different size, as was found by Shi et al. (2016) in a similar context, but including rotation. They found the dynamo to be more efficient in taller boxes, and interpreted this by having “cut out” some modes in the smaller boxes. However, determining the vertical wavenumber of the fastest growing mode in the kinematic stage for the decimated forcing runs, we find no evidence for this. As the turbulence in the cases with standard and decimated forcing is different though, we cannot regard this as completely conclusive evidence that rules out this scenario.

3.3. *Interpretation of the dynamo instability*

For SC driven dynamos, the dispersion relation from linear stability analysis for solutions, exponential in time, reads (see, e.g., Brandenburg et al. 2008)

$$\frac{\lambda_\pm}{\eta_{\rm T} k_z^2} = -1 \pm \frac{1}{\eta_{\rm T}} \sqrt{\left(\frac{S}{k_z^2} + \eta_{xy}\right) \eta_{yx} + \epsilon^2}, \tag{23}$$

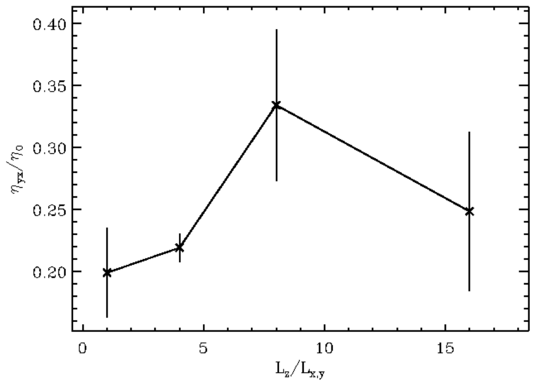

Figure 5. Dependence of η_{yx} on the aspect ratio $\mathcal{A}$ for SMHD cases with standard kinetic and magnetic forcing.

with $\eta_{\rm T} = \eta + \eta_{\rm t}$, $\eta_{\rm t} = (\eta_{xx} + \eta_{yy})/2$, $\epsilon = (\eta_{xx} - \eta_{yy})/2$. A necessary and sufficient condition for growing solutions is that the radicand is positive, and larger than $\eta_{\rm T}^2$. In other words (for $\epsilon \approx 0$)

$$D_{\eta S} \equiv \left(\frac{S}{k_z^2} + \eta_{xy}\right) \frac{\eta_{yx}}{\eta_{\rm T}^2} > 1. \tag{24}$$

Equation (23) is often further simplified by ignoring the contribution from η_{xy}, as it is considered negligible in comparison to S/k_z^2. This also holds for the systems studied here, but we note that η_{xy}, in all cases studied here, is much larger than η_{yx}, and in the kinetically forced cases even comparable to the diagonal components. Hence, setting it to zero, as has been done in some fitting experiments to determine the turbulent transport coefficients (see, e.g., Shi et al. 2016), is not justified. Also, especially in the magnetically forced cases, the η tensor becomes highly anisotropic, in which case the assumption $\epsilon \approx 0$, also often made in fitting experiments (Shi et al. 2016), breaks down in the strong shear regime, too.

For incoherent α–shear driven dynamos, the relevant dynamo number reads (see, e.g., Brandenburg et al. 2008)

$$D_{\alpha S} = \frac{\alpha_{\rm rms} \, |S|}{\eta_{\rm T}^2 k_z^3}, \tag{25}$$

where usually only the fluctuations of α_{yy} are considered for $\alpha_{\rm rms}$. They determined the critical $D_{\alpha S}$ to be ≈ 2.3 for white–noise α fluctuations. Squire & Bhattacharjee (2015) argued that an incoherent α–shear scenario should not lead to amplification of a mean magnetic field unless the diagonal components of $\boldsymbol{\alpha}$ would be markedly larger than the off-diagonals. Although this was not so in the moderate shear case, studied by Brandenburg et al. (2008), we have now clearly identified such a situation, both in kinetically and magnetically forced SMHD cases, see Figure 3. Hence the

Table 3. Dynamo numbers for the runs in Table 1.

Run	$k_z L_z/2\pi$	$D_{\eta S}$	$D_{\eta_{\rm rms} S}$	$D_{\alpha S}$
FK1a	1*	-1.4	1.6	2.8
FK1b	1	-3.9	5.3	19.2
FK8a	9*	-1.0	1.1	0.7
FK8b	9	-2.8	3.2	4.7
SK1a	1	0.1	0.3	2.9
SK1b	1	2.7	4.2	25.5
SK4a	4	0.1	0.2	1.5
SK4b	4	1.3	2.6	14.6
SK8a	4	0.5	0.7	8.2
SK8b	9	2.1	2.4	3.6
SKM1a	1*	-2.7	3.3	6.8
SKM4a	4*	-2.9	3.0	3.0
SKM8a	4*	-12.2	12.7	13.1
SKM16a	9*	-9.4	9.9	7.5
SKM1ad	1	-4.0	7.2	19.6
SKM4ad	4	-3.4	4.1	9.8
SKM8ad	8	-5.7	6.1	6.8

Runs marked with * are not dynamo active, hence the wavenumber of the growing dynamo mode is extracted from other runs of similar aspect ratio.

possibility of an incoherent α–shear dynamo cannot be ruled out for our simulations.

Brandenburg et al. (2008) also discussed the possibility of a contribution from an incoherent SC effect by fluctuations of η_{yx}. They studied a model, where both incoherent effects were acting together, the incoherent α effect mainly through α_{yy} while the incoherent SC effect was described by a dynamo number

$$D_{\eta_{\rm rms} S} = \frac{\eta_{yx,{\rm rms}}\,|S|}{\eta_{\rm T}^2 k_z^2}. \qquad (26)$$

They found that for small $D_{\eta_{\rm rms} S}$ the critical dynamo number, detected for the incoherent α effect alone, was not much altered while for higher values that critical number could be much reduced. Hence, to decide which dynamo effect is at play in systems with large fluctuations, one should always consider the dynamo numbers for both incoherent effects simultaneously.

Moreover, the presence of a coherent SC effect can alter the dynamo excitation condition which we now account for by adding a coherent induction term from η_{yx} to the simplified zero-dimensional (0-D) dynamo model of Brandenburg et al. (2008); see their Appendix C. We have verified that dynamo action in the 0-D model without any incoherent effects takes place when $D_{\eta S}$ is exceeding unity, as expected from the stability criterion (24). We compute new stability maps in the $D_{\eta_{\rm rms} S} - D_{\alpha S}$ plane for a series of dynamo numbers $D_{\eta S}$, in the range $[-1.5, 2]$. These values are similar in magnitude as those realized in our simulations, although not covering the extremal values obtained in the magnetic forcing cases. These are shown in Figure 6, where panels (d) and (e) closely match the stability map of the incoherent effects alone (compare with Figure 12 of Brandenburg et al. 2008). As expected, adding a coherent SC effect with a positive $D_{\eta S}$ enhances the dynamo instability, especially by lowering the critical dynamo number for the incoherent α–shear dynamo. This is seen through the shift of the stability line (white contours in Figure 6) to the left (towards smaller values of $D_{\alpha S}$) from (f) to (i). The incoherent SC dynamo threshold is also lowered, but the effect is more subtle, as seen through the much less dramatic shift of the stability boundary downwards (towards smaller values of $D_{\eta_{\rm rms} S}$) in Figure 6, panels (f)–(i). For $D_{\eta S} > 1$, the coherent SC effect alone would result in the excitation of a dynamo, but the presence of the incoherent effects cause small islands in which dynamo action is suppressed; see the dark red areas surrounded by the white contour in Figure 6, panels (g and h).

In the dynamo numbers (24)–(26) we also need the vertical wavenumber k_z of the dynamo mode which we determined from Fourier analysis of the mean fields during the kinematic phase of the dynamo. For those runs that are not dynamo active, we used k_z from a corresponding dynamo active run with higher ${\rm Re}_{\rm M}$ (for kinetically forced runs) or a different forcing function (for kinetically and magnetically forced runs), but the same aspect ratio; see Table 1, and denote those runs for which we obtained k_z from elsewhere with an asterisk. We also note that, if the dynamo enters saturation, the kinematically preferred mode is not necessarily any longer present. Independent of the aspect ratio of the box, all the saturated models exhibit a magnetic field at the scale of the box or, in other words, at the smallest permissible wavenumber.

In the FMHD cases, we obtain negative $D_{\eta S}$ and incoherent SC dynamo numbers of similar magnitude, with $D_{\alpha S}$ tending to be larger than $D_{\eta_{\rm rms} S}$, especially in Run FK1b. In the case of Run FK8a, no dynamo action is seen, and none of the dynamo numbers predict a dynamo either. In the other case without dynamo, Run FK1a, the η-related dynamo numbers predict no dynamo action, while $D_{\alpha S}$ alone would do so ($D_{\alpha S} = 2.8 > D_{\alpha S,{\rm crit}} = 2.3$). Its critical value, however, can be increased in this case, mainly by the presence of the rather strong coherent SC with a negative dynamo number. The two dynamo active cases have $D_{\alpha S}$ clearly above the critical value. Hence, the presence of moderate suppressing factors cannot prevent the dynamo instability. It clearly seems to be the incoherent α–shear one in the FMHD cases, because $D_{\eta S}$ is far too small in this case.

In the kinetically forced SMHD cases, however, η_{yx} is, negative, allowing for the possibility of a coherent SC dy-

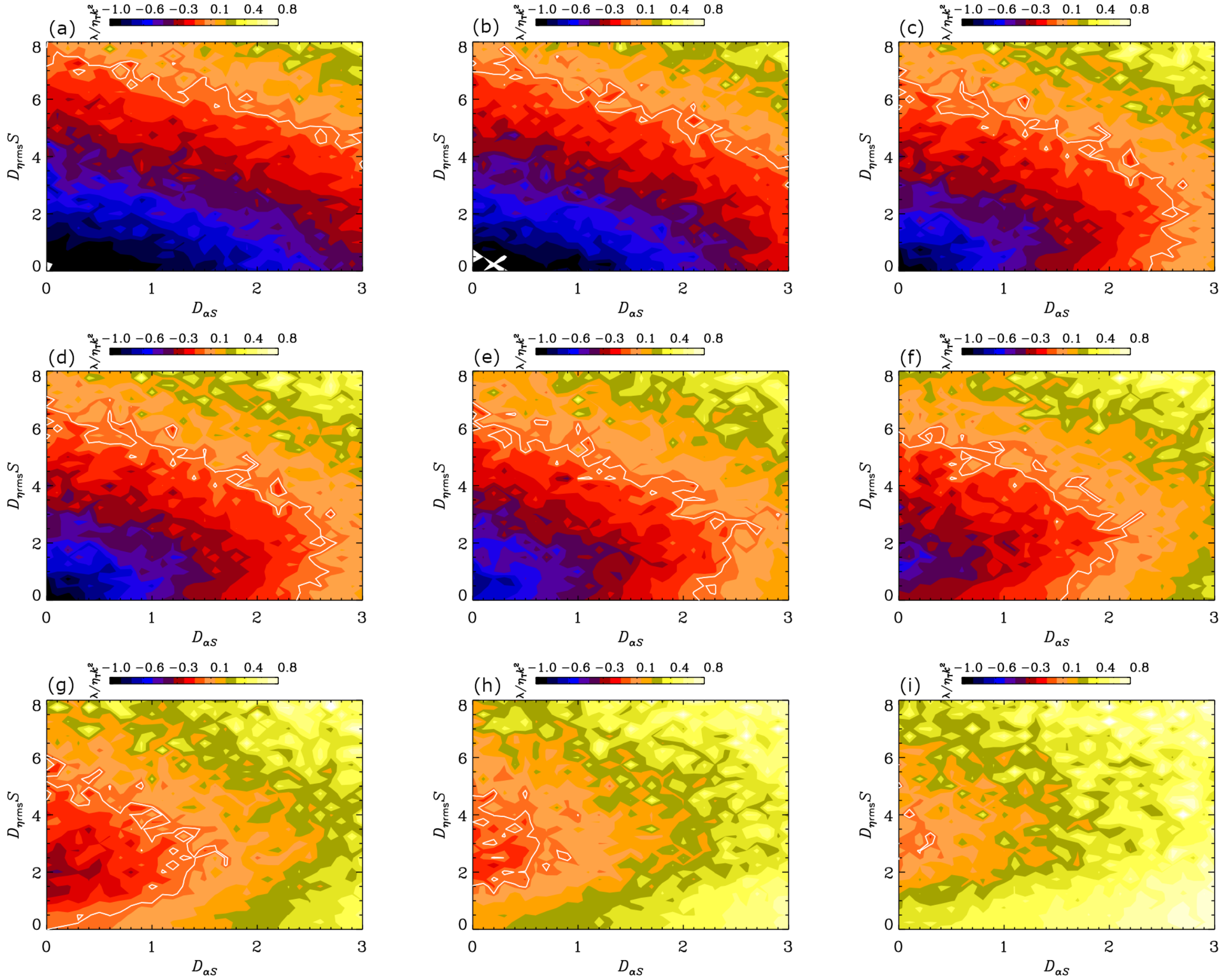

Figure 6. Stability diagrams for different values of $D_{\eta S}$: from top left to bottom right, -1.5,-1.0,-0.5,-0.1,0.1,0.5,1.0,1.5, and 2.0. White: zero–growth–rate contour.

namo. All our runs of this type are dynamo-active, but only the high Re_{M} cases exhibit supercritical $D_{\eta S}$ (> 1). Except for the case of Run SK4a, the $D_{\alpha S}$ and $D_{\eta_{\mathrm{rms}} S}$ values indicate supercriticality for the incoherent dynamo instabilities, explaining again most of our findings. Run SK4a has a low positive $D_{\eta S}$, but also the incoherent effects are well below their critical dynamo numbers. The coherent SC effect could, therefore, assist the dynamo, but this effect should be negligible according to the 0-D model. Hence, this dynamo remains unexplained with any dynamo scenario. Dynamo excitation is easier than in the FMHD cases, which might indicate that the coherent SC effect assists dynamo action favorably, but this could also be due to the SMHD simplifications.

In the kinetically and magnetically forced SMHD cases, the dynamo numbers indicate stability against the MSC effect, but are all, according to individual 0-D model runs (not presented here), supercritical for the incoherent dynamo effects, the incoherent SC effect being even more pronounced now than in the kinetically forced cases. Although the cases with standard forcing do not show exponential growth, their decimated forcing counterparts do so. Hence our interpretation here is that a dynamo is present in all the cases with kinetic and magnetic forcing. Even though the coherent SC effect now exhibits larger negative dynamo numbers we find, by running individual 0-D models, that in all cases it should not be able to damp the dynamo instability. Hence, again, the most likely mechanism for exciting the dynamo is the incoherent α–shear effect, with supercritical dynamo numbers in all cases. However, we cannot rule out the co-existence of an incoherent SC effect, as some runs also indicate supercriticality against it.

4. CONCLUSIONS

We have studied different types of sheared MHD systems with the quasi-kinematic (QKTFM) and non-linear (NLTFM) test-field methods. In those cases studied with the NLTFM, we simplified the MHD equations neglecting the pressure gradient in the momentum equation which allows us to ignore the equation for the fluctuating density in the test-field formulation, simplifying it somewhat. In the case of the full MHD equations studied with the QKTFM, we extend the previous results to even stronger shear, but still find no evidence for negative values of the η_{yx} component that could lead to LSD action through the SC effect.

In kinetically forced magnetized burgulence (SMHD), we measure negative values of η_{yx}. Indeed, dynamo action with both radial and azimuthal magnetic field components growing exponentially at the same rate is found. The dynamo numbers for the coherent and the incoherent effects, based on the measured turbulent transport coefficients, however, when employed in a simplified 0–D dynamo model, indicate that even in this case the dynamo is mainly driven by the incoherent α–shear effect, possibly assisted by the coherent SC effect one.

In the case of systems with standard magnetic forcing, we do not find exponential growth of the mean magnetic field. When we repeat this experiment with a decimated forcing function, removing the lowest wavenumbers, exponential growth is recovered. Hence, in our interpretation, there is still a dynamo instability in the magnetically forced cases, but it becomes engulfed by the rapid growth of the mean field due the presence of these low wavenumbers in the forcing, preventing us from seeing the exponential growth of the mean field. The measured η_{yx} are again positive, and increasing as a function of the magnitude of shear and the aspect ratio of the box, therefore incapable of driving a dynamo through the MSC effect. The computed dynamo numbers, compared against the 0-D model, again indicate the most likely driver of the dynamo to be the incoherent α–shear effect.

We acknowledge that the simplified MHD equations used here prevent our conclusions from being generally applicable. Hence we cannot fully reject the postulated possibility of a dynamo driven by the MSC effect. The measurements should be repeated with the full MHD equations, analyzed with a fully compressible TFM, also solving for the density fluctuations.

ACKNOWLEDGMENTS

We acknowledge fruitful and inspiring discussions with Dr. Jonathan Squire and Prof. Amitava Bhattacharjee in the Max Planck Princeton Center for Plasma Physics framework. M.J.K., M.R., and P.J.K. acknowledge the support of the Academy of Finland ReSoLVE Centre of Excellence (grant number 307411). P.J.K. acknowledges support from DFG Heisenberg grant (No. KA 4825/2-1). This project has received funding from the European Research Council (ERC) under the European Union's Horizon 2020 research and innovation programme (Project UniSDyn, grant agreement n:o 818665). A.B. acknowledges supported through the Swedish Research Council, grant 2019-04234, and the National Science Foundation under the grant AAG-1615100.

REFERENCES

Blackman, E. G. 2010, AN, 331, 101, doi: 10.1002/asna.200911304

Blackman, E. G., & Field, G. B. 2001, Physics of Plasmas, 8, 2407, doi: 10.1063/1.1351830

Brandenburg, A. 2001, ApJ, 550, 824, doi: 10.1086/319783

Brandenburg, A., Rädler, K. H., Rheinhardt, M., & Käpylä, P. J. 2008, ApJ, 676, 740, doi: 10.1086/527373

Brandenburg, A., Sokoloff, D., & Subramanian, K. 2012, SSRv, 169, 123, doi: 10.1007/s11214-012-9909-x

Brandenburg, A., & Subramanian, K. 2005, PhR, 417, 1, doi: 10.1016/j.physrep.2005.06.005

Cattaneo, F., & Vainshtein, S. I. 1991, ApJL, 376, L21, doi: 10.1086/186093

Chamandy, L., & Singh, N. K. 2018, MNRAS, 481, 1300, doi: 10.1093/mnras/sty2301

Devlen, E., Brandenburg, A., & Mitra, D. 2013, MNRAS, 432, 1651, doi: 10.1093/mnras/stt590

Elperin, T., Kleeorin, N., & Rogachevskii, I. 2003, PhRvE, 68, 016311, doi: 10.1103/PhysRevE.68.016311

Heinemann, T., McWilliams, J. C., & Schekochihin, A. A. 2011, PhRvL, 107, 255004, doi: 10.1103/PhysRevLett.107.255004

Hubbard, A., Del Sordo, F., Käpylä, P. J., & Brandenburg, A. 2009, MNRAS, 398, 1891, doi: 10.1111/j.1365-2966.2009.15108.x

Käpylä, P. J., Mitra, D., & Brandenburg, A. 2009, PhRvE, 79, 016302, doi: 10.1103/PhysRevE.79.016302

Käpylä, P. J., Rheinhardt, M., Brandenburg, A., & Käpylä, M. J. 2020, A&A, 636, A93, doi: 10.1051/0004-6361/201935012

Lanotte, A., Noullez, A., Vergassola, M., & Wirth, A. 1999, Geophysical and Astrophysical Fluid Dynamics, 91, 131, doi: 10.1080/03091929908203701

Lesur, G., & Ogilvie, G. I. 2008, A&A, 488, 451, doi: 10.1051/0004-6361:200810152

Marston, J. B., Conover, E., & Schneider, T. 2008, Journal of Atmospheric Sciences, 65, 1955, doi: 10.1175/2007JAS2510.1

Mitra, D., & Brandenburg, A. 2012, MNRAS, 420, 2170, doi: 10.1111/j.1365-2966.2011.20190.x

Pipin, V. V., & Seehafer, N. 2009, A&A, 493, 819, doi: 10.1051/0004-6361:200810766

Rädler, K. H. 1969a, Monats. Dt. Akad. Wiss., 11, 194

—. 1969b, Monats. Dt. Akad. Wiss., 11, 272

Rheinhardt, M., & Brandenburg, A. 2010, A&A, 520, A28, doi: 10.1051/0004-6361/201014700

—. 2012, Astronomische Nachrichten, 333, 71, doi: 10.1002/asna.201111625

Rogachevskii, I., & Kleeorin, N. 2003, PhRvE, 68, 036301, doi: 10.1103/PhysRevE.68.036301

—. 2004, PhRvE, 70, 046310, doi: 10.1103/PhysRevE.70.046310

Schrinner, M., Rädler, K.-H., Schmitt, D., Rheinhardt, M., & Christensen, U. 2005, Astron. Nachr., 326, 245, doi: 10.1002/asna.200410384

Schrinner, M., Rädler, K.-H., Schmitt, D., Rheinhardt, M., & Christensen, U. R. 2007, Geophysical and Astrophysical Fluid Dynamics, 101, 81, doi: 10.1080/03091920701345707

Shi, J.-M., Stone, J. M., & Huang, C. X. 2016, MNRAS, 456, 2273, doi: 10.1093/mnras/stv2815

Singh, N. K., & Jingade, N. 2015, ApJ, 806, 118, doi: 10.1088/0004-637X/806/1/118

Singh, N. K., & Sridhar, S. 2011, PhRvE, 83, 056309, doi: 10.1103/PhysRevE.83.056309

Squire, J., & Bhattacharjee, A. 2015, ApJ, 813, 52, doi: 10.1088/0004-637X/813/1/52

—. 2016, Journal of Plasma Physics, 82, 535820201, doi: 10.1017/S0022377816000258

Sridhar, S., & Singh, N. K. 2010, Journal of Fluid Mechanics, 664, 265, doi: 10.1017/S0022112010003745

—. 2014, MNRAS, 445, 3770, doi: 10.1093/mnras/stu1981

Sridhar, S., & Subramanian, K. 2009a, PhRvE, 79, 045305, doi: 10.1103/PhysRevE.79.045305

—. 2009b, PhRvE, 80, 066315, doi: 10.1103/PhysRevE.80.066315

Vainshtein, S. I., & Cattaneo, F. 1992, ApJ, 393, 165, doi: 10.1086/171494

Yousef, T. A., Heinemann, T., Schekochihin, A. A., et al. 2008, PhRvL, 100, 184501, doi: 10.1103/PhysRevLett.100.184501

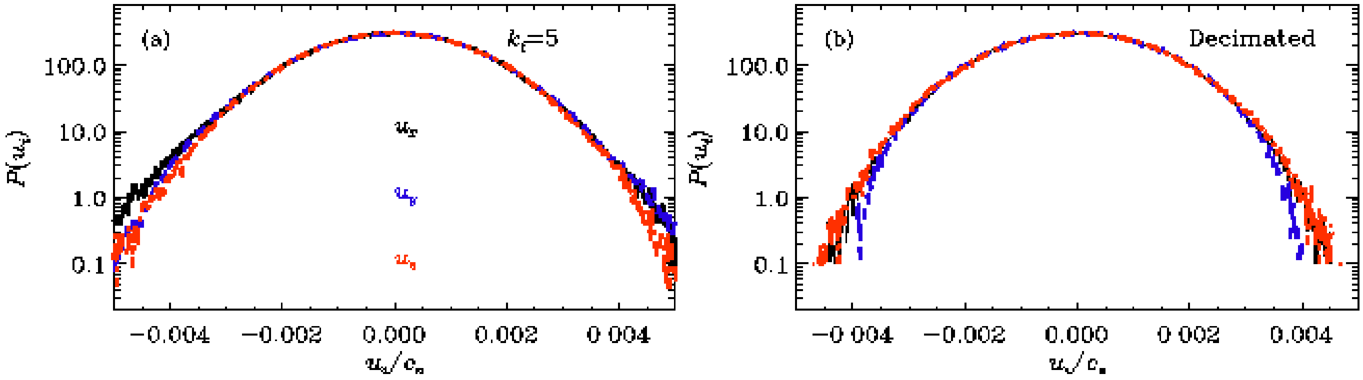

Figure 7. PDFs of all three velocity components from 64^3 shearless SMHD runs with $k_\mathrm{f} = 5$. (a): standard; (b): decimated forcing with $k_\mathrm{min}/k_1 = 2$. All pdfs are nearly Gaussians with kurtosis ~ 3.

Table 4. η tensor components measured with the different variants of NLTFM from Run SKM1a007.

Method	η_{xx}/η_0	η_{yy}/η_0	η_{yx}/η_0	η_{xy}/η_0
ju	2.110 ± 0.023	2.089 ± 0.007	0.112 ± 0.026	-0.208 ± 0.028
jb	2.276 ± 0.152	2.106 ± 0.020	0.124 ± 0.009	-0.212 ± 0.018
bb	2.297 ± 0.144	2.116 ± 0.018	0.129 ± 0.018	-0.188 ± 0.017
bu	2.155 ± 0.047	2.127 ± 0.017	0.113 ± 0.014	-0.212 ± 0.022

APPENDIX

A. COMPARISON OF STANDARD AND DECIMATED FORCING FUNCTIONS

To investigate the possible anisotropy due to the removal of all $|k_{x,y,z}|/k_1 \leq k_\mathrm{min}/k_1$ from the forcing (decimation), we perform two hydrodynamic simulations without shear. Both runs were performed with 64^3 grid points and $k_\mathrm{f}/k_1 = 5$, one without decimation and one with, using $k_\mathrm{min}/k_1 = 2$. All other parameters were the same and u_rms was similar in the two cases. In Figure 7 we show probability density functions (PDFs) of the three components of $\boldsymbol{u}$ from a snapshot of each run. These PDFs are normalized such that $\int P(u_i)\,\mathrm{d}u_i = 1$. We find that the PDFs of u_x, u_y, and u_z are in both cases on top of each other suggesting that the stochastic flows are nearly isotropic, at least in a statistical sense.

Furthermore, we define a dimensionless quantity $\zeta(\theta,\phi) = \sqrt{\langle(\boldsymbol{u}\cdot\hat{\boldsymbol{n}})^2\rangle}/u_\mathrm{rms}$, with $\hat{\boldsymbol{n}} = (\sin\theta\cos\phi,\, \sin\theta\sin\phi,\, \cos\theta)$, which is useful to assess the degree of anisotropy, where θ and ϕ are the polar and azimuthal angles, respectively, as in a spherical coordinate system. Figure 8 shows snapshots of $\zeta(\theta,\phi)$ which reveal anisotropic features, both in the standard (undecimated) and the decimated case. However, at least in the undecimated case the flows are expected to be statistically isotropic when data from a large number of snapshots are combined, as there is no preferred direction in the system. We show the variation of ζ as a function of ϕ at two fixed values of θ (45° and 90°) in Figure 9, after performing an average over eight snapshots. As expected, the degree of anisotropy decreased compared to a single snapshot; it is below 7% as inferred from the values of ζ in Figure 9. We also notice an $m = 2$ modulation which is more pronounced in the decimated case, likely due to gaps in the thin k shell around k_f. The statistical isotropy of the flow is expected to be improved further at higher resolution and when data from a longer time-series are combined.

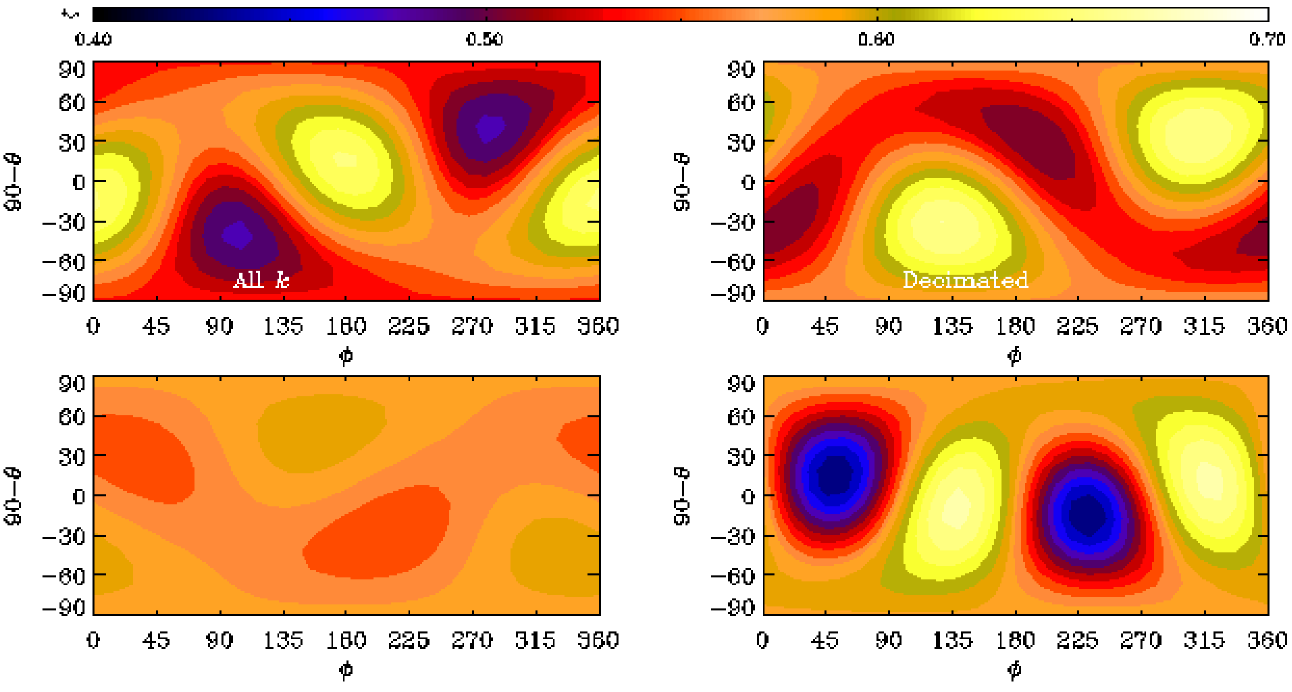

Figure 8. Two snapshots (top/bottom) of $\zeta = \sqrt{\langle(\boldsymbol{u}\cdot\hat{\boldsymbol{n}})^2\rangle}/u_{\rm rms}$, in the $\theta\phi$ plane. Left: undecimated; right: decimated with $k_{\rm min}/k_1 = 2$.

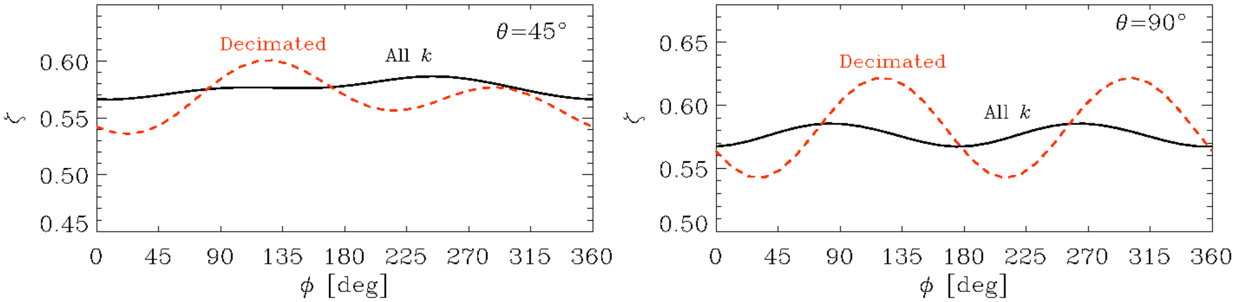

Figure 9. Variation of ζ with the azimuthal angle ϕ at polar angles $\theta = 45°$ (left) and $90°$ (right), after averaging over 8 snapshots. Solid/black: undecimated; dashed/red: decimated with $k_{\rm min}/k_1 = 2$.

B. COMPARISON AND VALIDATION OF THE NLTFM

B.1. *Comparison of the different variants of the NLTFM*

As is described in Rheinhardt & Brandenburg (2010), with respect to the terms $\boldsymbol{u}\times\boldsymbol{b}$ and $\boldsymbol{j}\times\boldsymbol{b}$ there are four possibilities to define the NLTFM, depending on how one combines the fluctuating fields from the main run, $\boldsymbol{u}$, $\boldsymbol{b}$, $\boldsymbol{j}$ with the test solutions $\boldsymbol{u}_{\overline{B}}$, $\boldsymbol{b}_{\overline{B}}$, $\boldsymbol{j}_{\overline{B}}$. These variants were denoted as ju (using $\boldsymbol{j}$ and $\boldsymbol{u}$ in the pondero- and electromotive forces, respectively), jb (using $\boldsymbol{j}$ and $\boldsymbol{b}$), bu (using $\boldsymbol{b}$ and $\boldsymbol{u}$), and bb (using $\boldsymbol{b}$ in both). Further variants due to the term $\boldsymbol{u}\cdot\boldsymbol{\nabla}\boldsymbol{u}$ are not considered here. Previously it was concluded that the ju method would be the most stable one (Rheinhardt & Brandenburg 2010). Here we examine how the different variants behave in SMHD with standard (random) forcing. The results for Run SKM1a007 are listed in Table 4 and depicted in Figure 10, showing the η_{xx} component obtained with all four variants. We can see that jb and bb produce measurements that are nearly identical at any phase of the simulation. The measurements with bu deviate from these occasionally, but the largest

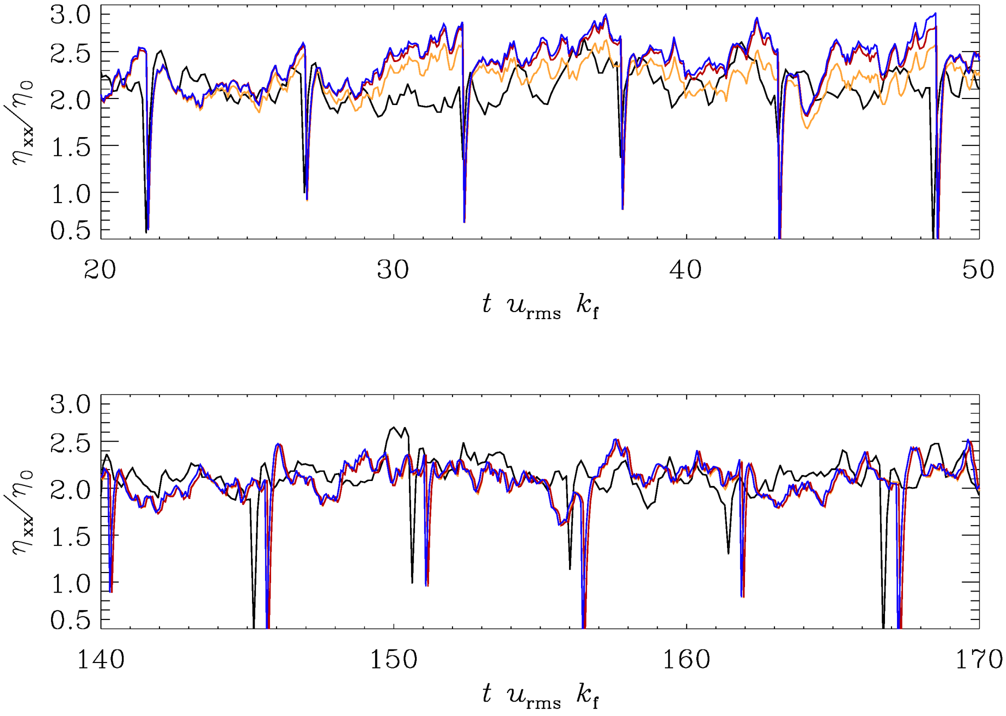

Figure 10. Time evolution of η_{xx} from Run SKM1a007 with the four variants of the NLTFM. Black: ju, blue: bb, orange: bu, red: jb. Upper panel: early stages, lower panel: late stages of the simulation.

deviations occur for ju. While the three former variants tend to produce turbulent transport coefficients that clearly grow within the resetting intervals, ju produces plateaus, this difference being especially pronounced in Figure 10, top panel. This is indicative of the test problems getting unstable during the resetting interval, which can lead to overestimation of and increased uncertainties in the measured transport coefficients. With the resetting time of 50 (in code units) in most of our simulations, however, the measured differences between the variants were very small, but nevertheless we observed a tendency of the tensor components to be larger in magnitude when jb and bb were used; see also Table 4. Hence, throughout the paper we use the ju variant which produces measurements with clearer plateaus in the turbulent transport coefficients.

B.2. *Kinetically forced SMHD analyzed with QKTFM and NLTFM*

To further validate the NLTFM, we perform runs of kinetically forced SMHD, and measure the turbulent transport coefficients with both QKTFM and NLTFM. We compare them in two regimes: one where the magnetic field is very weak, and another where the magnetic field is already dynamically significant. We choose the setup SK4b, and show our results in Figure 11 in terms of η_{yx} as function of time. Although some differences due to the randomness of the forcing have to be expected, we observe a very good agreement between the two methods.

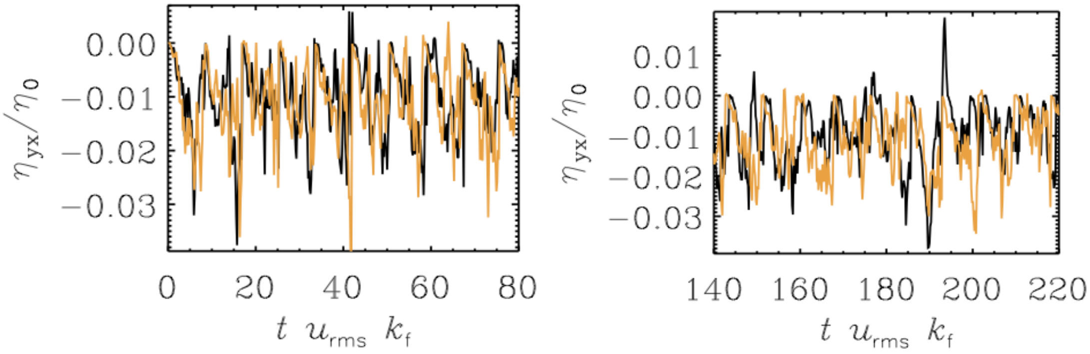

Figure 11. Time evolution of η_{yx} from Run SK4b with QKTFM (orange) and NLTFM (black). Measurements from a stage, when the dynamo field is still weak (left) and dynamically significant (right).